A State-Space Approach to Optimal Level-Crossing Prediction for Linear Gaussian Processes

Rodney A. Martin, *Member, IEEE*

***Abstract*—In this paper, approximations of an optimal level-crossing predictor for a zero-mean stationary linear dynamical system driven by Gaussian noise in state-space form are investigated. The study of this problem is motivated by the practical implications for design of an optimal alarm system, which will elicit the fewest false alarms for a fixed detection probability in this context. This work introduces the use of Kalman filtering in tandem with the optimal level-crossing prediction problem. It is shown that there is a negligible loss in overall accuracy when using approximations to the theoretically optimal predictor, at the advantage of greatly reduced computational complexity.**

***Index Terms*—Alarm systems, approximation methods, Kalman filtering, level-crossing problems, prediction methods.**

I. Introduction

THIS paper introduces a novel approach of combining the practical appeal of Kalman filtering with the design of an optimal alarm system for the prediction of level-crossing events. A comprehensive demonstration of practical application for the design of optimal alarm systems has been covered in the literature [1]–[5]. The background theory for optimal alarm systems preceded this work, and was introduced by a small subset of these authors [6], [7]. However, the latter is by no means a comprehensive list, and illustrates only a cross section of the primary authors responsible for introducing optimal alarm systems in a classical and practical sense.

It was shown by Svensson [1] and Svensson *et al.* [2] that an optimal alarm system can be constructed by finding relevant alarm system metrics (as are used in ROC curve analysis) as a function of a design parameter by way of an optimal alarm condition. The optimal alarm condition is fundamentally an alarm region or decision boundary based upon a likelihood ratio criterion via the Neyman–Pearson lemma, as shown in [6], [7]. This allows for the design of an optimal alarm system that will elicit the fewest possible false alarms for a fixed detection probability. This becomes important when considering the numerous applications that might benefit from an intelligent tradeoff between false alarms and missed detections.

Manuscript received March 31, 2007; revised November 17, 2009. Date of current version September 15, 2010. This work was supported in part by the Integrated Vehicle Health Management (IVHM) project, funded by the Aviation Safety Program of NASA's Aeronautics Research Mission Directorate.

The author is with the Intelligent Systems Division and the Intelligent Data Understanding Group, NASA Ames Research Center, Moffett Field, CA 94035-0001 USA (e-mail: rodney.martin@nasa.gov).

Communicated by A. Host-Madsen, Associate Editor for Detection and Estimation.

Color versions of one or more of the figures in this paper are available online at http://ieeexplore.ieee.org.

Digital Object Identifier 10.1109/TIT.2010.2059930

In general, the design of optimal alarm systems demonstrates practical potential to enhance reliability and support health management for space propulsion, civil aerospace applications, and other related fields. Due to the great costs, not to mention potential dangers associated with a false alarm due to evasive or extreme action taken as a result of false indications, there are great opportunities for cost savings/cost avoidance, and enhancement of overall safety. Nonetheless, the intent of this paper is to demonstrate the utility of optimal level-crossing prediction from a more theoretical perspective.

Due to the fact that optimal alarm regions cannot be expressed in closed form, one of the aims of this study is to investigate approximations for the design of an optimal alarm system. The resulting metrics can easily be compared to competing methods that may also provide some level of predictive capability, but have no provision for minimizing false alarms for the prediction of level-crossing events.

There are several examples of level-crossing events to be studied, varying from a simple one-sided case to a more complicated two-sided case. The former one-sided case involves exceedances and/or upcrossings of a single level spanning two adjacent time points for a discrete-time process. This is the case that has traditionally been studied in previous work and invokes ARMA(X) prediction methods [1], [2], [5]–[7]. The latter two-sided case involves a level crossing event that may span many time points and exceed upper and lower levels symmetric about the mean of the process many times during this timeframe.

A variant of the latter more complicated two-sided case has been investigated by Kerr [8] and uses a Kalman filter-based approach. The two-sided case is more practically relevant when monitoring residuals that may be derived from the output of other machine learning algorithms or transformed parameters that relate to system performance. The two-sided case is investigated here, and a Kalman filter-based approach is used in an optimal manner relevant for the prediction of level-crossings.

The prediction of such a level-crossing event is also very similar to what has been established as the state of the art for newly minted spacecraft engines, as studied in [9]; however, no guarantees of optimality exist. This provides additional practical motivation for investigating a level crossing event that spans many time steps, moving beyond what has previously been studied in this vein.

There is an extensive history of invoking Kalman-filter-based approaches within the failure detection literature. A comprehensive survey of such techniques can be found in a book by Basseville and Nikiforov [10], which cites groundbreaking articles by Willsky and Jones [11], and Kerr [8]. More recently, the Kalman filter has been used to address the level-crossing

U.S. Government work not protected by U.S. copyright.

prediction problem in application to condition monitoring [12], but without any theoretical guarantees of optimality. A competitor to the optimal alarm system is described in [13], and uses adaptive optimal on-line techniques in a Bayesian formulation, providing more modeling flexibility. However, there are still considerable computational issues with such an approach, and a well-defined cost function is still required, even when the posterior probability is adaptively updated.

Relevant alarm system metrics such as ones used in ROC curve analysis can be expressed as a function of a design parameter via an optimal alarm condition. These same metrics will act as the basis for comparison to competing methods to be presented in Section II-C. These competing methods may provide some level of predictive capability, but have no provision for minimizing false alarms. The optimal level-crossing predictor uses an optimal alarm condition in order to provide an upper bound on false alarm probability. All of these techniques are leveraged to predict another distinctly more critical level-crossing event (based upon an extreme value given by the critical level, L), and may provide a viable alternative to the use of a *single* level based solely upon a decision rule as is used with methods such as CUSUM, SPRT, GLR, *etc.*

However, CUSUM, SPRT, GLR, *etc.*, as well as the optimal level-crossing predictor are all fundamentally based upon the application of the Neyman–Pearson lemma and resulting decision rule. As such, they are *all* optimally guaranteed an upper bound on false alarm probability for a maximal detection probability under certain technical conditions related to the hypotheses being tested. The primary difference between these methods is in the characterization of the null hypotheses and application of the resulting optimal decision rule. For the optimal level-crossing predictor, the null hypothesis integrates the definition of a critical event, which can be constructed such that multiple level-crossings of an extreme value span multiple time steps into the future, implicitly enabling a predictive capability for alarm system design. For the other methods such as CUSUM, SPRT, GLR, *etc.*, null or alternate hypotheses are constructed to target the detection of abrupt changes in model parameters. These methods are also the one most commonly found in the literature, *e.g.*, [14], [8], [11], [15], and [10].

Operating under the alternate paradigm, a critical event can be constructed to emulate the adverse conditions requiring prediction in the context of an extreme value level-crossing rather than an abrupt change in model parameters. The distinction between these two paradigms is one of the most discernable differences in the theoretical techniques used here and in other literature derived from extreme value theory, [1]–[3], [5]–[7]. The use of an optimal level-crossing predictor is naturally parameterized to allow for prediction of an event occurring in the future. Thus, this technique should perform well in practice for early prediction, conditioned on the use of alarm system parameters that are well characterized by the modeling assumptions. Overall, this paper aims to more precisely close the gap between the use of Kalman filtering and optimal alarm systems. Although motivated by fault detection and prediction, recognizing that the literature in this area is quite expansive, this paper aims to shed light on a segment of the literature that has been largely overlooked.

TABLE I
SUMMARY OF MATHEMATICAL NOTATION

Mathematical Representation	*Nomenclature*
$\succeq$	Positive semi-definite
$(\bullet)'$	Not (Set complement)
$\mathcal{I}$	Universe of all events
$(\bullet)^\top$	Transpose
$P(\bullet)$	Probability
$E[\bullet]$ or $\mu_\bullet$	Expected Value
$\hat{\bullet}_{k+j\|k}$	$E[\bullet\|y_0,\ldots,y_k]$ (Conditional Expectation)
$\tilde{\bullet}_k$	Orthonormal rotation of $\bullet_k$ in vector space
$\bullet^*$	Result of vector space orthonormal rotation in probability or event space
$\mathcal{N}(\mu,\Sigma)$	Gaussian distribution with mean μ and covariance Σ
$\mathcal{N}(\mathbf{x};\mu,\Sigma)$	Gaussian distribution evaluated at $\mathbf{x}$ with mean μ and covariance Σ

II. METHODOLOGY

A level-crossing event is defined with a critical level, L, that is assumed to have a fixed, static value. The level is exceeded by some critical parameter than can be represented by a dynamic process, and is often modeled as a zero-mean stationary linear dynamical system driven by Gaussian noise. Most of the theory that follows is based upon this standard representation of the optimal level-crossing problem. As such, it is an underlying assumption that measured or transformed data can be fitted well to a model represented by a linear dynamical system driven by Gaussian noise. The state-space formulation is shown in (1)–(3), demonstrating propagation of both the state, $\mathbf{x}_k \in \mathbb{R}^n$ which is corrupted by process noise $\mathbf{w}_k \in \mathbb{R}^n$, and the state covariance matrix, $\mathbf{P}_k$, which evolve with the time-invariant system matrix $\mathbf{A}$. The output, $y_k \in \mathbb{R}$ is univariate, and is corrupted by measurement noise $v_k \in \mathbb{R}$

$$\mathbf{x}_{k+1} = \mathbf{A}\mathbf{x}_k + \mathbf{w}_k \tag{1}$$

$$y_k = \mathbf{C}\mathbf{x}_k + v_k \tag{2}$$

$$\mathbf{P}_{k+1} = \mathbf{A}\mathbf{P}_k\mathbf{A}^\top + \mathbf{Q} \tag{3}$$

where

$$\mathbf{w}_k \sim \mathcal{N}(\mathbf{0},\mathbf{Q}),\ \ \mathbf{Q} \succeq \mathbf{0}$$
$$v_k \sim \mathcal{N}(0,R),\ \ R > 0$$
$$\mathbf{x}_0 \sim \mathcal{N}(\mu_{\mathbf{x}},\mathbf{P}_0).$$

A summary of the basic mathematical notation not defined elsewhere is provided in Table I. There is great flexibility in constructing a mathematical representation for the level-crossing event, C_k. Ostensibly, the target application will drive the definition of this event. As such, in this paper the event of interest is shown in (4), *cf.* Kerr [8] in consideration of the motivating factors described in the introduction. This level-crossing event represents at least one exceedance outside of the threshold envelope specified by $[-L, L]$ of the process y_k within the specified look-ahead prediction window, d

$$C_k \triangleq \bigcup_{j=1}^{d} S_{k+j} = \bigcup_{j=1}^{d} E'_{k+j} = \mathcal{I} \setminus \bigcap_{j=1}^{d} E_{k+j} \tag{4}$$

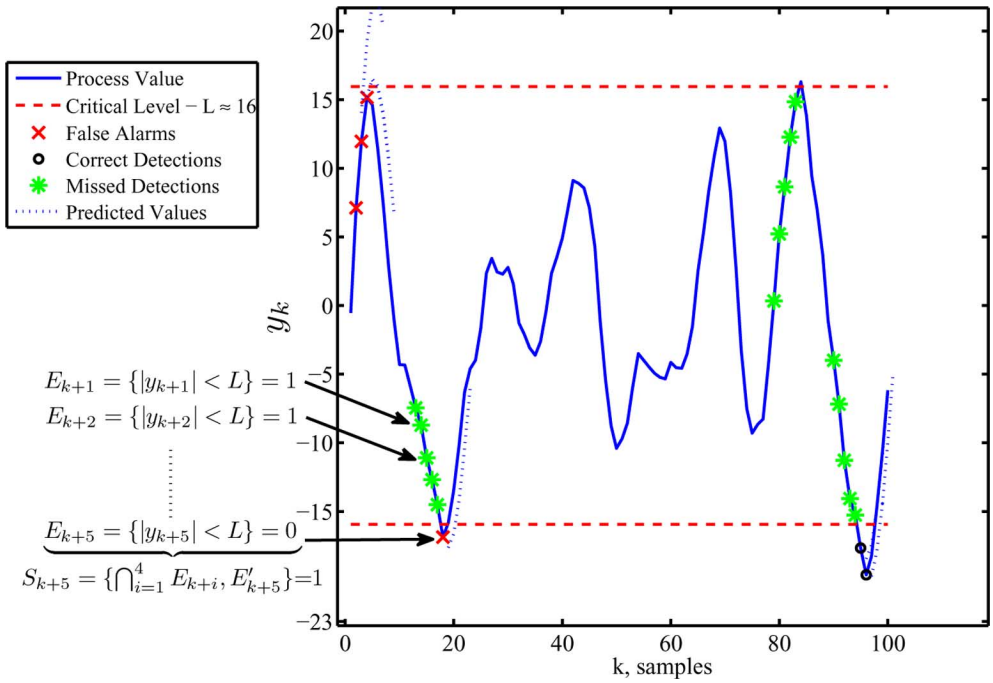

Fig. 1. Level-crossing event realization.

where

$$E_{k+j} \triangleq \{|y_{k+j}| < L\},\ \forall\, j \geq 1$$
$$S_{k+j} \triangleq \begin{cases} E'_{k+j} & j = 1 \\ \bigcap_{i=1}^{j-1} E_{k+i}, E'_{k+j} & \forall\, j > 1. \end{cases}$$

Fig. 1 illustrates the relationship between subevents S_{k+j} and E_{k+j}, when $j = 5$. The event C_k can be represented as the union of disjoint subevents, S_{k+j}, or as the union of overlapping subevents, E'_{k+j}. However, due to DeMorgan's theorem, the latter can be expressed in a more compact fashion via a *single* term when computing the probability of the overall event. This obviates the need for using the inclusion/exclusion rule to compute the event probability based upon the union of overlapping subevents, E'_{k+j}, where the number of terms would be exponential in d. It also obviates the need for computing the probability based upon the former union of disjoint subevents, S_{k+j}, where there is no need for use of the inclusion/exclusion rule. However, the number of terms would still be linear in d, as the probability computation of the union of disjoint subevents is represented by the sum of terms involving S_{k+j}. Equation (5) represents the unconditional probability of the level-crossing event in its most compact representational form

$$P(C_k) = 1 - \int_{-L}^{L} \cdots \int_{-L}^{L} \mathcal{N}(\mathbf{y}_d; \mu_{\mathbf{y}_d}, \Sigma_{\mathbf{y}_d}) d\mathbf{y}_d \qquad (5)$$

where

$$\mathbf{y}_d \triangleq \begin{bmatrix} y_{k+1} \\ \vdots \\ y_{k+d} \end{bmatrix},\ \mu_{\mathbf{y}_d} = \mathbf{0}_d = \begin{bmatrix} 0 \\ \vdots \\ 0 \end{bmatrix}$$
$$\Sigma_{\mathbf{y}_d} \triangleq \begin{cases} \mathbf{C}\mathbf{P}_k\mathbf{C}^\top + R & \forall\, i = j \in [1, \ldots, d] \\ \mathbf{C}\mathbf{P}_{k+i,k+j}\mathbf{C}^\top & \forall\, j > i \in [1, \ldots, d] \end{cases}$$

and $\mathbf{P}_{k+i,k+j} \triangleq \mathbf{A}^j(\mathbf{P}_k - \mathbf{P}_{ss}^L)(\mathbf{A}^\top)^i + \mathbf{A}^{j-i}\mathbf{P}_{ss}^L$.

$\Sigma_{\mathbf{y}_d}$ can be approximated as shown in (6) by substituting the steady-state version of the Lyapunov equation given previously as (3), $\mathbf{P}_{ss}^L$, in place of $\mathbf{P}_k$, which agrees with the assumption of stationarity

$$\Sigma_{\mathbf{y}_d} \approx \begin{cases} \mathbf{C}\mathbf{P}_{ss}^L\mathbf{C}^\top + R & \forall\, i = j \in [1, \ldots, d] \\ \mathbf{C}\mathbf{A}^{j-i}\mathbf{P}_{ss}^L\mathbf{C}^\top & \forall\, j > i \in [1, \ldots, d] \end{cases}. \qquad (6)$$

This approximation, while it introduces error with regards to the probability of a level-crossing event, $P(C_k)$ at a specific point in time, k, is ostensibly negligible and will provide for a great computational advantage in the design of an alarm system. Instead of designing an alarm system for each time step, a single alarm system is designed for all time steps. The approximation is based upon the limiting statistics that are reached at steady-state, which greatly reduces the computational burden. The steady-state assumption has not been used in work by Antunes *et al.* [13], but doing so also incurs much greater computational effort.

Theorem 1, which can be found in Section VII, provides the mathematical underpinnings for the optimal alarm condition corresponding to the level-crossing event, shown here as (7). Alternatively, the optimal alarm condition derived in Theorem 1 can be expressed in terms of the subevents E_{k+j}, as shown in (8)

$$P(C_k | y_0, \ldots, y_k) \geq P_b \qquad (7)$$
$$\Leftrightarrow P\left(\bigcap_{j=1}^{d} E_{k+j} | y_0, \ldots, y_k\right) \leq 1 - P_b. \qquad (8)$$

The optimal alarm condition has, therefore, been derived from the use of the likelihood ratio resulting in the conditional inequality as given in (7). This basically says "give alarm when the conditional probability of the event, C_k, exceeds the level P_b." Here, P_b represents some optimally chosen border or threshold probability with respect to a relevant alarm system

metric. It is necessary to find the alarm regions in order to design the alarm system. This alarm region is parameterized by future process output predictions and covariances, which can be derived from the standard Kalman filter (9)–(14)

$$\hat{y}_{k|k} = \mathbf{C}\hat{\mathbf{x}}_{k|k} \tag{9}$$
$$\hat{\mathbf{x}}_{k+1|k} = \mathbf{A}\hat{\mathbf{x}}_{k|k} \tag{10}$$
$$\hat{\mathbf{x}}_{k+1|k+1} = \hat{\mathbf{x}}_{k+1|k} + \mathbf{F}_{k+1|k}\varepsilon_{k+1} \tag{11}$$
$$\mathbf{F}_{k+1|k} \triangleq \mathbf{P}_{k+1|k}\mathbf{C}^{\top}(\mathbf{C}\mathbf{P}_{k+1|k}\mathbf{C}^{\top} + R)^{-1} \tag{12}$$
$$\mathbf{P}_{k+1|k} = \mathbf{A}\mathbf{P}_{k|k}\mathbf{A}^{\top} + \mathbf{Q} \tag{13}$$
$$\mathbf{P}_{k+1|k+1} = \mathbf{P}_{k+1|k} - \mathbf{F}_{k+1|k}\mathbf{C}\mathbf{P}_{k+1|k} \tag{14}$$

where

$$\hat{\mathbf{x}}_{k|k} \triangleq E[\mathbf{x}_k|y_0,\ldots,y_k]$$
$$\mathbf{P}_{k|k} \triangleq E[(\mathbf{x}_k - \hat{\mathbf{x}}_{k|k})(\mathbf{x}_k - \hat{\mathbf{x}}_{k|k})^T|y_0,\ldots,y_k]$$
$$\varepsilon_k \triangleq y_k - \mathbf{C}\hat{\mathbf{x}}_{k|k-1}.$$

Relevant predictions, covariances and cross covariances are given below as (15)–(19), respectively

$$\hat{y}_{k+j|k} = \mathbf{C}\mathbf{A}^{j}\hat{\mathbf{x}}_{k+j|k} \tag{15}$$
$$\mathbf{P}_{k+j|k} = \mathbf{A}^{j}(\mathbf{P}_{k|k} - \mathbf{P}^{L}_{ss})(\mathbf{A}^{\top})^{j} + \mathbf{P}^{L}_{ss} \tag{16}$$
$$\approx \mathbf{A}^{j}(\hat{\mathbf{P}}^{R}_{ss} - \mathbf{P}^{L}_{ss})(\mathbf{A}^{\top})^{j} + \mathbf{P}^{L}_{ss} \tag{17}$$
$$\mathbf{P}_{k+i,k+j|k} = \mathbf{A}^{j}(\mathbf{P}_{k|k} - \mathbf{P}^{L}_{ss})(\mathbf{A}^{\top})^{i} + \mathbf{A}^{j-i}\mathbf{P}^{L}_{ss} \tag{18}$$
$$\approx \mathbf{A}^{j}(\hat{\mathbf{P}}^{R}_{ss} - \mathbf{P}^{L}_{ss})(\mathbf{A}^{\top})^{i} + \mathbf{A}^{j-i}\mathbf{P}^{L}_{ss} \tag{19}$$
$$\hat{\mathbf{P}}^{R}_{ss} = \mathbf{P}^{R}_{ss} - \mathbf{F}_{ss}\mathbf{C}\mathbf{P}^{R}_{ss} \tag{20}$$
$$\mathbf{F}_{ss} = \mathbf{P}^{R}_{ss}\mathbf{C}^{\top}(\mathbf{C}\mathbf{P}^{R}_{ss}\mathbf{C}^{\top} + R)^{-1}. \tag{21}$$

$\mathbf{P}^{R}_{ss}$ is the combined steady-state version of (13) and (14) given previously, or the discrete algebraic Riccati equation, and $\hat{\mathbf{P}}^{R}_{ss}$ is the steady-state *a posteriori* covariance matrix given in (20). Equation (21) is also used in (20), which is the steady-state version of the Kalman gain from (12).

The approximations shown in (17) and (19) will provide a computational advantage in designing the optimal alarm system and its corresponding approximations for reasons stated previously. Due to the approximation of $\mathbf{P}_{k|k}$ with $\hat{\mathbf{P}}^{R}_{ss}$ shown in these equations, the Kalman filter will be suboptimal, as cited by Lewis [16]. However, the assumption of stationarity is required for the design of an optimal alarm system as defined by Theorem 1, and holds here as well.

A more formal representation of the optimal alarm region is shown in (22), which essentially defines a sublevel set of $g(\hat{\mathbf{y}}_d) \triangleq P\left(\bigcap_{j=1}^{d} E_{k+j}|y_0,\ldots,y_k\right)$ as a function of $\hat{\mathbf{y}}_d$

$$A_k \triangleq \left\{\bigcap_{i=1}^{d}\hat{y}_{k+i|k} : P(C_k|y_0,\ldots,y_k) \geq P_b\right\}$$
$$\triangleq \left\{\bigcap_{i=1}^{d}\hat{y}_{k+i|k} : P\left(\bigcap_{j=1}^{d} E_{k+j}|y_0,\ldots,y_k\right) \leq 1 - P_b\right\}. \tag{22}$$

Equations (23)–(24) give the multivariate normal probability computation to be performed via numerical integration, required for enabling the optimal alarm condition

$$P\left(\bigcap_{j=1}^{d} E_{k+j}|y_0,\ldots,y_k\right) = \int_{-L}^{L}\cdots\int_{-L}^{L}\mathcal{N}(\mathbf{y}_d;\hat{\mathbf{y}}_d,\hat{\Sigma}_{\mathbf{y}_d})d\mathbf{y}_d \tag{23}$$
$$= \int_{-L-\hat{y}_{k+1|k}}^{L-\hat{y}_{k+1|k}}\cdots\int_{-L-\hat{y}_{k+d|k}}^{L-\hat{y}_{k+d|k}} \times \mathcal{N}(\mathbf{y}_d;\mathbf{0}_d,\hat{\Sigma}_{\mathbf{y}_d})d\mathbf{y}_d \tag{24}$$

where

$$\hat{\mathbf{y}}_d \triangleq E[\mathbf{y}_d|y_0,\ldots,y_k] = \begin{bmatrix}\hat{y}_{k+1|k}\\ \vdots \\ \hat{y}_{k+d|k}\end{bmatrix}$$
$$\hat{\Sigma}_{\mathbf{y}_d} \triangleq \begin{cases} V_{k+i|k} & \forall\, i = j \in [1,\ldots,d] \\ \mathbf{C}\mathbf{P}_{k+i,k+j|k}\mathbf{C}^{\top} & \forall\, i \neq j \in [1,\ldots,d]\end{cases}$$
$$V_{k+i|k} \triangleq \mathbf{C}\mathbf{P}_{k+i|k}\mathbf{C}^{\top} + R.$$

The feasible region for values of P_b can easily be determined by applying an intermediate value theorem from calculus which provides sufficient conditions for finding a level set solution. The sufficient conditions are shown as (25)–(26), and the resulting level set is shown as (27)

$$g(\mu_{\mathbf{y}_d}) \geq 1 - P_b \tag{25}$$
$$\lim_{|\hat{\mathbf{y}}_d|\setminus\hat{y}_{k+j|k}\to\infty} g(\hat{\mathbf{y}}_d) < 1 - P_b,\ \forall\, j \in [1,\ldots,d] \tag{26}$$
$$L_A \triangleq \left\{\bigcap_{j=1}^{d}\hat{y}_{k+j|k} : g(\hat{\mathbf{y}}_d) = 1 - P_b\right\}. \tag{27}$$

The notation that represents the limiting condition shown in (26) is $|\hat{\mathbf{y}}_d| \setminus \hat{y}_{k+j|k} \to \infty$, and is meant to indicate that all elements of $\hat{\mathbf{y}}_d$ other than $\hat{y}_{k+j|k}$ approach $\pm\infty$. Application of this condition yields $P_b < 1$, which is true by definition, and application of the sufficient condition shown in (25) yields $P_b \geq 1 - g(\mu_{\mathbf{y}_d})$. Thus, the feasible region for P_b is $P_b \in [1 - g(\mu_{\mathbf{y}_d}), 1]$.

It is not possible to obtain a closed-form representation of the parametrization for the optimal alarm region shown in (22). As such, a Monte Carlo approach must be used. This allows the ROC curve statistics to be estimated empirically with observational and truth data generated from the existing model and corresponding simulations of level-crossing events.

However, with the aid of two distinct approximations, ROC curve statistics can be generated by numerically integrating expressions for the computation of relevant multivariate normal probabilities. These multivariate probability computations are performed by using an adaptation of Genz's algorithm [17], which is based upon a robust and computationally efficient technique designed to be used for integrations in multiple dimensions for multivariate normal distributions. This provides a tool necessary for the design of approximations to an optimal alarm system, and also other failure detection algorithms such as the

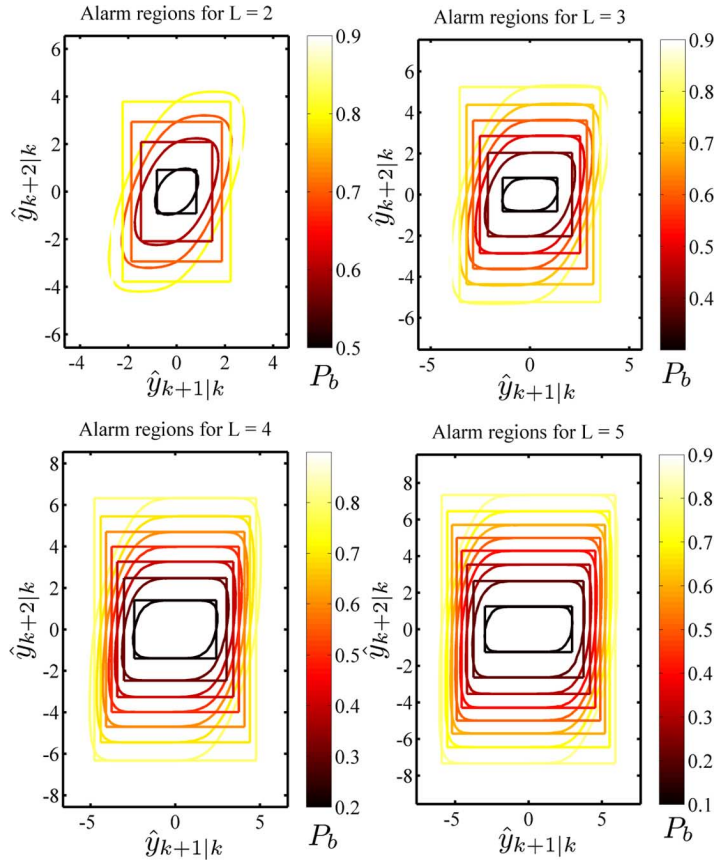

Fig. 2. Root-finding approximations for optimal alarm region.

one most often used by Kerr [18], who specifically cites issues with the computation of these types of integrals. As such, computationally intensive simulation runs using Monte-Carlo empirical estimation can be avoided.

A. Root-Finding Approximation

The optimal alarm region, A_k, can be approximated by the alarm region specified by $\bigcup_{j=1}^{d} \Omega_{A_j}$. Fundamentally, the approximation is constructed by solving for asymptotic bounds on the exact alarm region. By using asymptotes, a geometrical approximation is implicitly formed with a hyperbox around the alarm region. Simple 2-D examples of such hyperboxes for various values of L, and P_b are shown in Fig. 2. There is visual evidence that limiting effects for this approximation exist, as both L and P_b approach the extremities of their feasible domains. The limiting effects of P_b will be given thorough theoretical treatment in this paper, but the limiting effects of L will be investigated in earnest in a sequel paper, and only touched on briefly in Section IV.

Mathematically, the approximation is formed by solving a root-finding problem which yield bounding asymptotes. The root-finding problem is posed by first taking the limit as each dimension of (22) approaches the respective dimension of $\mu_{\mathbf{y}_d}$, other than the one for which the asymptote is being derived. Equation (28) expresses this limiting condition as a function of the dimension of interest

$$f(\hat{y}_{k+j|k}) \triangleq \lim_{\hat{\mathbf{y}}_d \setminus \hat{y}_{k+j|k} \to \mu_{\mathbf{y}_d} \setminus \mu_{y_{k+j}}} P\left(\bigcap_{j=1}^{d} E_{k+j} | y_0, \ldots, y_k \right). \tag{28}$$

Having defined $f(\hat{y}_{k+j|k})$, it is now possible to express Ω_{A_j} in (29)–(30)

$$\Omega_{A_j} = \left\{ \hat{y}_{k+j|k} : f(\hat{y}_{k+j|k}) \leq 1 - P_b \right\} \tag{29}$$

$$= \left\{ |\hat{y}_{k+j|k}| \geq L_{A_j} \right\} \tag{30}$$

where the root-finding problem is given by numerically solving (31)

$$L_{A_j} \triangleq \left\{ |\hat{y}_{k+j|k}| : f(\hat{y}_{k+j|k}) = 1 - P_b \right\}. \tag{31}$$

Thus, the root-finding approximation to the optimal alarm region is given by $\bigcup_{j=1}^{d} \Omega_{A_j} \approx A_k$. Note that the function f incorporates all elements of the covariance matrix $\hat{\Sigma}_{\mathbf{y}_d}$ when computing the asymptotes, just as when constructing the sublevel set for the the exact optimal alarm region. Furthermore, the feasible region for P_b is identical to the sublevel set of the exact optimal alarm region, $P_b \in [1 - g(\mu_{\mathbf{y}_d}), 1] \equiv [1 - \min_j f(\mu_{y_{k+j}}), 1]$ by using a similar argument and set of sufficient conditions, as shown in (32)–(33) below

$$f(\mu_{y_{k+j}}) \geq 1 - P_b, \quad \forall j \in [1, \ldots, d] \tag{32}$$

$$\lim_{|\hat{y}_{k+j|k}| \to \infty} f(\hat{y}_{k+j|k}) < 1 - P_b, \quad \forall j \in [1, \ldots, d] \tag{33}$$

However, there is one primary difference between this approximation and the exact alarm region. The conditional mean, $\hat{\mathbf{y}}_d$, associated with the asymptotic approximation is parameterized only by the corresponding dimension of the conditional

mean, $\hat{y}_{k+j|k}$, whereas the exact optimal alarm region uses all dimensions of the distribution simultaneously.

It is possible to generate formulae for the true and false positive rates as a function of L_{A_j} by appealing to (34)–(35), where in place of A_k its approximation $\bigcup_{j=1}^{d} \Omega_{A_j}$ may be used.

- True positive rate:

$$P_d = P(C_k|A_k) = \frac{P(C_k, A_k)}{P(A_k)}. \tag{34}$$

- False positive rate:

$$\begin{aligned} P_{fa} = P\left(A_k|C_k'\right) &= \frac{P(C_k', A_k)}{P(C_k')} \\ &= \frac{P(A_k) - P(C_k, A_k)}{1 - P(C_k)}. \end{aligned} \tag{35}$$

The formula for $P(C_k)$ has already been introduced in (5), and holds regardless of the alarm system approximation being used. Thus, only the additional expressions for $P(C_k, A_k)$ and $P(A_k)$ given in (36)–(37) are necessary for computing P_d and P_{fa}. These equations use $P_{b_{\text{crit}}} \triangleq 1 - g(\mu_{\mathbf{y}_d}) = 1 - \min_j f(\mu_{y_{k+j}})$, and are also implicitly expressed as a function of the design parameter, P_b, as a consequence of (31). Note also that the off-diagonal blocks of the covariance matrix $\Sigma_{\mathbf{z}}$ are equivalent to $\hat{\Sigma}_{\hat{\mathbf{y}}_d}$ as a consequence of the projection theorem

$$\begin{aligned} P(A_k) &= \begin{cases} P\left(\bigcup_{j=1}^{d} \Omega_{A_j}\right) & P_b > P_{b_{\text{crit}}} \\ 1 & P_b = P_{b_{\text{crit}}} \end{cases} \\ &= \begin{cases} 1 - P\left(\bigcap_{j=1}^{d} \Omega'_{A_j}\right) & P_b > P_{b_{\text{crit}}} \\ 1 & P_b = P_{b_{\text{crit}}} \end{cases} \end{aligned} \tag{36}$$

$$P(C_k, A_k) = \begin{cases} P(C_k) - P(A_k') + P(C_k', A_k') & P_b > P_{b_{\text{crit}}} \\ P(C_k) & P_b = P_{b_{\text{crit}}} \end{cases} \tag{37}$$

where

$$\begin{aligned} P(A_k') &= P\left(\bigcap_{j=1}^{d} \Omega'_{A_j}\right) = P\left(\bigcap_{j=1}^{d} |\hat{y}_{k+j|k}| < L_{A_j}\right) \\ &= \int_{-L_{A_1}}^{L_{A_1}} \cdots \int_{-L_{A_d}}^{L_{A_d}} \mathcal{N}(\hat{\mathbf{y}}_d; \mu_{\mathbf{y}_d}, \hat{\Sigma}_{\hat{\mathbf{y}}_d}) d\mathbf{y}_d \end{aligned}$$

and

$$\begin{aligned} \hat{\Sigma}_{\hat{\mathbf{y}}_d} &\triangleq \Sigma_{\mathbf{y}_d} - \hat{\Sigma}_{\mathbf{y}_d} \\ &= \mathbf{O}\left(\mathbf{P}_{ss}^{L} - \mathbf{P}_{ss}^{R}\right)\mathbf{O}^{\top} \\ \mathbf{O} &\triangleq \begin{bmatrix} \mathbf{C} \\ \vdots \\ \mathbf{C}\mathbf{A}^{d-1} \end{bmatrix}. \end{aligned}$$

Furthermore

$$\begin{aligned} P(C_k', A_k') &= P\left(\bigcap_{j=1}^{d} E_{k+j}, \bigcap_{j=1}^{d} \Omega'_{A_j}\right) \\ &= \int_{-L}^{L} \cdots \int_{-L}^{L} \int_{-L_{A_1}}^{L_{A_1}} \cdots \int_{-L_{A_d}}^{L_{A_d}} \\ &\quad \times \mathcal{N}(\mathbf{z}; \mu_{\mathbf{z}}, \Sigma_{\mathbf{z}}) d\mathbf{z} \end{aligned}$$

where

$$\begin{aligned} \mathbf{z} &\triangleq \begin{bmatrix} \mathbf{y}_d \\ \hat{\mathbf{y}}_d \end{bmatrix} \\ \mu_{\mathbf{z}} &\triangleq \begin{bmatrix} \mu_{\mathbf{y}_d} \\ \mu_{\mathbf{y}_d} \end{bmatrix} \\ \Sigma_{\mathbf{z}} &\triangleq \begin{bmatrix} \Sigma_{\mathbf{y}_d} & \hat{\Sigma}_{\hat{\mathbf{y}}_d} \\ \hat{\Sigma}_{\hat{\mathbf{y}}_d} & \hat{\Sigma}_{\hat{\mathbf{y}}_d} \end{bmatrix}. \end{aligned}$$

B. Closed-Form Approximation

The optimal alarm region, A_k, can also be approximated by an alarm region specified by $\bigcup_{j=1}^{d} A_k^j$, with a successive approximation on A_k^j; A_k^j is defined in (38). Fundamentally, the approximation can be constructed in the same fashion as the root-finding method, by solving for asymptotic bounds on the exact alarm region

$$A_k^j = \left\{\hat{y}_{k+j|k} : P(E_{k+j}|y_0, \ldots, y_k) \leq 1 - P_b\right\}. \tag{38}$$

A containment relationship between the exact optimal alarm region and the union of approximate subregions $\bigcup_{j=1}^{d} A_k^j \subseteq A_k$ can easily be shown with a linear transformation of the conditionally defined Gaussian vector $\mathbf{y}_d$ to a vector of independent variables. The integrand of (24) is a multivariate Gaussian density whose conditional covariance matrix is given by $\hat{\Sigma}_{\mathbf{y}_d}$. The orthonormal decomposition of this covariance matrix and density of the corresponding transformed vector $\tilde{\mathbf{y}}_d$ are shown in (39)–(41)

$$\tilde{\mathbf{y}}_d = \Lambda \mathbf{y}_d \tag{39}$$

$$\hat{\Sigma}_{\mathbf{y}_d} = \Lambda \Gamma \Lambda^{\top} \tag{40}$$

$$\mathcal{N}(\mathbf{y}_d; \mathbf{0}_d, \hat{\Sigma}_{\mathbf{y}_d}) = \mathcal{N}(\tilde{\mathbf{y}}_d; \mathbf{0}_d, \Gamma). \tag{41}$$

Here, the elements of $\tilde{\mathbf{y}}_d$ are independent, and thus, Γ is diagonal. As such, geometric containment easily follows when considering a revised expression for A_k and $\bigcup_{j=1}^{d} A_k^j$. Thus, the latter approximation to the exact alarm region can be rewritten in the transformed probability space as shown in (42). Note that this expression does not change significantly from what was given in (38)

$$\bigcup_{j=1}^{d} A_k^j = \bigcup_{j=1}^{d} \left\{\hat{y}_{k+j|k} : P(E_{k+j}^*|\tilde{y}_0, \ldots, \tilde{y}_k) \leq 1 - P_b^*\right\}. \tag{42}$$

The exact alarm region A_k can be rewritten in the transformed probability space as shown in (43); however, the expression changes significantly, and in such a manner to allow for direct comparison to (42)

$$\begin{aligned} A_k &= \left\{\bigcap_{i=1}^{d} \hat{y}_{k+i|k} : P\left(\bigcap_{j=1}^{d} E_{k+j}^*|\tilde{y}_0, \ldots, \tilde{y}_k\right) \leq 1 - P_b^*\right\} \\ &= \left\{\bigcap_{i=1}^{d} \hat{y}_{k+i|k} : \prod_{j=1}^{d} P\left(E_{k+j}^*|\tilde{y}_0, \ldots, \tilde{y}_k\right) \leq 1 - P_b^*\right\}. \end{aligned} \tag{43}$$

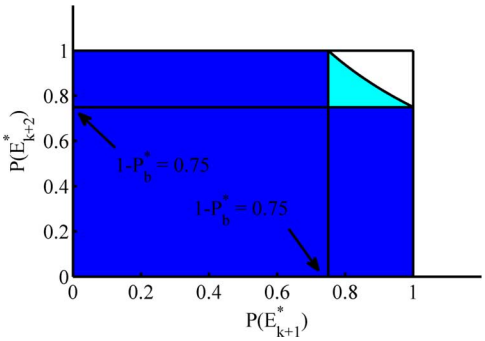

Fig. 3. Containment of the approximation by exact alarm region in transformed probability space.

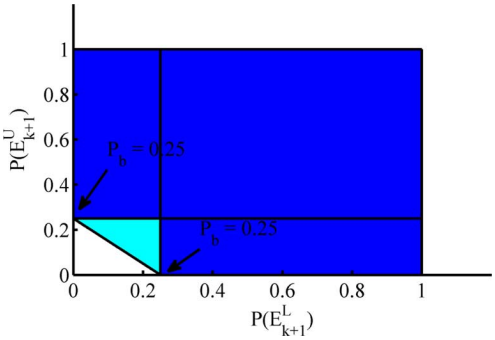

Fig. 4. Closed-form approximation in probability space.

Because containment in this probability space is invariant under orthonormal rotations, it follows from (42) and (43), that $\bigcup_{j=1}^{d} A_k^j \subseteq A_k$, so that the approximate alarm region is a proper subset of the exact alarm region. Fig. 3 provides illustrative evidence of this containment in the transformed probability space when $d = 2$. Here, the union of the light and dark colored sections represents A_k (formula shown below) and the dark colored section represents the approximation $A_k^1 \cup A_k^2$

$$A_k = \Big\{ (\tilde{y}_{k+1|k}, \tilde{y}_{k+2|k}) : P(E^*_{k+1}|\tilde{y}_0, \ldots, \tilde{y}_k) \cdot P(E^*_{k+2}|\tilde{y}_0, \ldots, \tilde{y}_k) \le 1 - P_b^* \Big\}.$$

A successive approximation is required in order to obtain a closed-form representation and parametrization of the alarm region without having to resort to root-finding required for solving $P(E_{k+j}|y_0, \ldots, y_k) \le 1 - P_b$, which is equivalent to $P(|y_{k+j}| > L|y_0, \ldots, y_k) \ge P_b$. This second approximation is given by (44), which breaks this condition containing an absolute value into constitutive inequalities

$$A_k^{i,j} = \Big\{ \hat{y}_{k+j|k} : P({E^i_{k+j}}'|y_0, \ldots, y_k) \ge P_b \Big\} \tag{44}$$

where

$$\begin{aligned} i \in \mathcal{B} \equiv \{\ell, \upsilon\} &= \{\text{lower limit, upper limit}\} \\ E^{\upsilon}_{k+j} &= \{y_{k+j} < L\} \\ E^{\ell}_{k+j} &= \{y_{k+j} > -L\}. \end{aligned}$$

Thus, $P\left({E^{\upsilon}_{k+j}}'|y_0, \ldots, y_k\right) + P\left({E^{\ell}_{k+j}}'|y_0, \ldots, y_k\right) \ge P_b$ is approximated by two distinct inequalities given by the union of $P\left({E^{\upsilon}_{k+j}}'|y_0, \ldots, y_k\right) \ge P_b$ and $P\left({E^{\ell}_{k+j}}'|y_0, \ldots, y_k\right) \ge P_b$. This subsequent approximation can easily be visualized in Fig. 4. The union of the light and dark colored sections shown in Fig. 4, represents A_k^1. Thus, the dark colored section alone from Fig. 4 is a subset of this area, such that $A_k^{\upsilon,1} \cup A_k^{\ell,1} \subseteq A_k^1$. If Fig. 4 is replicated for $j \in [1, \ldots, d]$, then it becomes clear that more generally (45) holds, which summarizes all of the containment relationships for the approximations covered in this subsection

$$\bigcup_{j=1}^{d} \bigcup_{i \in \mathcal{B}} A_k^{i,j} \subseteq \bigcup_{j=1}^{d} A_k^j \subseteq A_k. \tag{45}$$

By using this successive approximation, the alarm region can now be represented in "closed-form," as shown in (46) below

$$\begin{aligned} \bigcup_{j=1}^{d} \bigcup_{i \in \mathcal{B}} A_k^{i,j} &= \bigcup_{j=1}^{d} |\hat{y}_{k+j|k}| \\ &\ge L + \sqrt{V_{k+j|k}}\Phi^{-1}(P_b) \equiv L_{A_j}. \end{aligned} \tag{46}$$

$\Phi^{-1}(\cdot)$ represents the inverse cumulative normal standard distribution function, and L_{A_j} represents the limits of integration, $\forall\, j \in [1, \ldots, d]$. The L_{A_j} values can now been re-defined to replace the integration limits used for the root-finding method in (34)–(37). As such, these same equations are valid for computing P_d and P_{fa} in order to construct an ROC curve using this "closed-form" approximation as well. However, in place of A_k when using these equations, the approximation $\bigcup_{j=1}^{d} \bigcup_{i \in \mathcal{B}} A_k^{i,j}$ is used.

The domain of feasibility for this approximation now changes, and $P_{b_{\text{crit}}}$ takes on a new value, which differs from identical values of $P_{b_{\text{crit}}} = 1 - g(\mu_{\mathbf{y}\,d})$ and $P_{b_{\text{crit}}} = 1 - \min_j f(\mu_{y_{k+j}})$ corresponding to the feasibility regions for the optimal alarm region and the root-finding approximation, respectively. A derivation for the new value of $P_{b_{\text{crit}}}$ is provided in (47)–(51) below. The derivation is based upon the premise that $L_{A_j} > 0$, where the last step from (50) to (51) uses Lemmas 2-5 which can be found in Section VII, and the fact that $R > 0$

$$L_{A_j} > 0 \,\forall\, j \in [1, \ldots, d] \tag{47}$$

$$L + \sqrt{V_{k+j|k}}\Phi^{-1}(P_b) > 0 \,\forall\, j \in [1, \ldots, d] \tag{48}$$

$$\bigcap_{j=1}^{d} P_b > \Phi\left(\frac{-L}{\sqrt{V_{k+j|k}}}\right) \triangleq P_{b_j} \tag{49}$$

$$P_{b_{\text{crit}}} = \max_j P_{b_j} \tag{50}$$

$$= \Phi\left(\frac{-L}{\sqrt{V_{k+d|k}}}\right) = P_{b_d}. \tag{51}$$

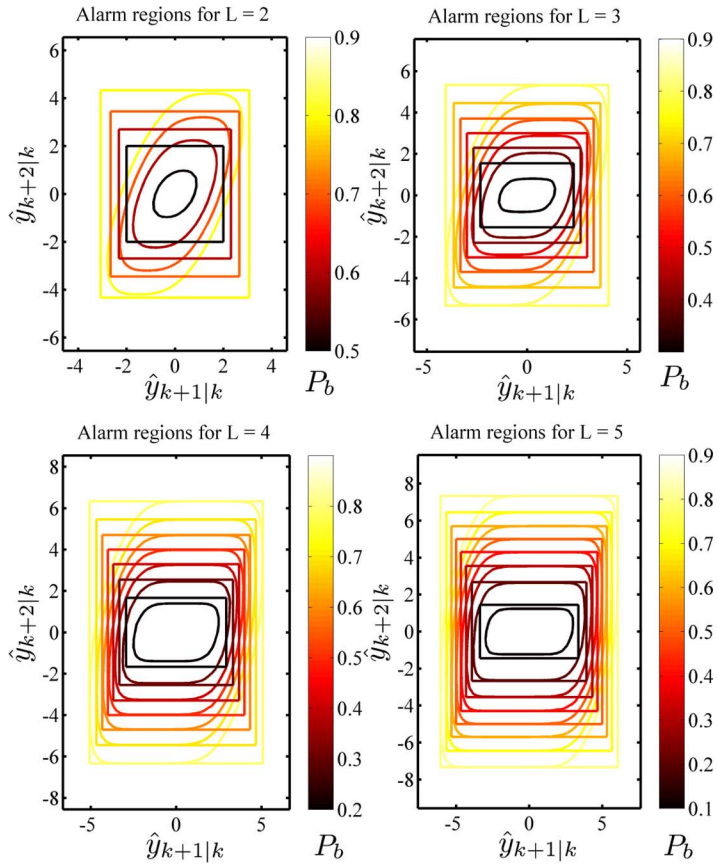

Fig. 5. Closed-form approximations for optimal alarm region.

Again, by using asymptotes a geometrical approximation is implicitly formed with a hyperbox around the alarm region. As before, simple 2-D examples of such hyperboxes for various values of L and P_b are shown in Fig. 5. Furthermore, just as for the root-finding approximation, visual evidence that limiting effects for this approximation also exist, as both L and P_b approach the extremities of their feasible domains. Note that both the approximation represented by Fig. 3 and the successive approximation represented by Fig. 4 have been applied to yield the vector space result shown in Fig. 5. Both Figs. 3 and 5 have been illustrated for the case when $d = 2$.

Due to the containment relationship labeled (45), qualitative arguments for the under-reporting of P_d and P_{fa} can be made for this approximation. A less aggressive, more optimistic strategy will result in comparison to the exact optimal method. It is unclear if this approximation will be more or less accurate than the previous root-finding approximation. However, the off-diagonal elements of the covariance matrix $\hat{\Sigma}_{\mathbf{y}_d}$ are not used for computing the asymptotes of this "closed-form" approximation. Recall that the root-finding method incorporates all elements of the covariance matrix when computing the asymptotes. Yet both methods use asymptotic approximations which are parameterized only by the corresponding dimension of the conditional mean, $\hat{y}_{k+j|k}$.

As is apparent intuitively from Figs. 2 and 5, $A_k^j \subseteq \Omega_{A_j}$, thus $\bigcup_{j=1}^{d} A_k^j \subseteq \bigcup_{j=1}^{d} \Omega_{A_j}$. It is clear from visual comparison of these figures that this containment relationship exists between the root-finding and "closed-form" approximations. For a mathematical proof of this containment, recall (29)–(30) for Ω_{A_j}, shown again below, and compare them to (38) for A_k^j, also shown again below

$$\begin{aligned}\Omega_{A_j} &= \{\hat{y}_{k+j|k} : f(\hat{y}_{k+j|k}) \leq 1 - P_b\} \\ &= \{|\hat{y}_{k+j|k}| \geq L_{A_j}\} \\ A_k^j &= \{\hat{y}_{k+j|k} : P(E_{k+j}|y_0, \ldots, y_k) \leq 1 - P_b\}.\end{aligned}$$

Examining the regions of integration for $f(\hat{y}_{k+j|k})$ and $P(E_{k+j}|y_0, \ldots, y_k)$, as shown in (52)–(56) below, it is evident that a clear containment relationship exists

$$\begin{aligned} & f(\hat{y}_{k+j|k}) \\ &= \lim_{\hat{\mathbf{y}}_d \setminus \hat{y}_{k+j|k} \to \mu_{\mathbf{y}_d} \setminus \mu_{y_{k+j}}} P\left(\bigcap_{j=1}^{d} E_{k+j}|y_0, \ldots, y_k\right) \quad (52) \\ &= \int_{\mathcal{D}_\Omega} \mathcal{N}(\mathbf{y}_d; \hat{\mathbf{y}}_d, \hat{\Sigma}_{\mathbf{y}_d}) d\mathbf{y}_d \quad (53) \\ &= \int_{-L}^{L} \cdots \int_{-L-\hat{y}_{k+j|k}}^{L-\hat{y}_{k+j|k}} \cdots \int_{-L}^{L} \\ &\quad \mathcal{N}(\mathbf{y}_d; \hat{\mathbf{y}}_d, \hat{\Sigma}_{\mathbf{y}_d}) d\mathbf{y}_d \quad (54) \\ & P(E_{k+j}|y_0, \ldots, y_k) \\ &= \int_{\mathcal{D}_A} \mathcal{N}(\mathbf{y}_d; \hat{\mathbf{y}}_d, \hat{\Sigma}_{\mathbf{y}_d}) d\mathbf{y}_d \quad (55) \\ &= \int_{-\infty}^{\infty} \cdots \int_{-L-\hat{y}_{k+j|k}}^{L-\hat{y}_{k+j|k}} \cdots \int_{-\infty}^{\infty} \\ &\quad \mathcal{N}(\mathbf{y}_d; \hat{\mathbf{y}}_d, \hat{\Sigma}_{\mathbf{y}_d}) d\mathbf{y}_d \quad (56) \end{aligned}$$

where

$$\begin{aligned}\mathbb{X} &= \{[-L, L]\} \subset \mathbb{R}\\ \mathcal{D}_\Omega &= \left\{\mathbb{X}^{d-1} \times [-L - \hat{y}_{k+j|k}, L - \hat{y}_{k+j|k}]\right\}\\ \mathcal{D}_A &= \left\{\mathbb{R}^{d-1} \times [-L - \hat{y}_{k+j|k}, L - \hat{y}_{k+j|k}]\right\}.\end{aligned}$$

It is clear that $\mathcal{D}_\Omega \subseteq \mathcal{D}_A$ due to the fact that $\mathbb{X}^{d-1} \subseteq \mathbb{R}^{d-1}$. As such, $f(\hat{y}_{k+j|k}) \leq P(E_{k+j}|y_0, \ldots, y_k)$ easily follows due to the fact that both expressions share a common integrand. It is, therefore, evident that the original claim $A_k^j \subseteq \Omega_{A_j}$, and thus $\bigcup_{j=1}^d A_k^j \subseteq \bigcup_{j=1}^d \Omega_{A_j}$ is mathematically sound.

According to this newly derived containment relationship, and by again using qualitative arguments, it is clear that the root-finding approximation will be more aggressive, and less optimistic than the closed form approximation. However, there is no containment relationship that can be established between the root-finding method and the exact optimal alarm region as could be performed for the closed form approximation. As such, even though the root-finding method incorporates all elements of the covariance matrix when computing its asymptotes, this approximation strategy may be overly aggressive and overshoot the performance of the exact optimal method under certain circumstances. This mathematical intuition will be supported by demonstrating this effect with examples in Section IV.

C. Redline and Predictive Alarm Systems

Two baseline "redline" and "predictive" alarm systems will be compared to the optimal alarm system and its approximations. All methods will attempt to predict the level-crossing event defined by (4). The redline alarm system attempts to define an envelope, $[-L_A, L_A]$, outside of which an alarm will be triggered to forewarn of the impending level-crossing event. The probabilities necessary to compute P_d and P_{fa} based upon (34)–(35) for this alarm system are provided in (57)–(60), where a redefinition of $A_k = \{|y_k| > L_A\}$ now holds, such that the alarm is based only on the current process value

$$P(A_k) = P(|y_k| > L_A) \tag{57}$$

$$= 2\Phi\left(\frac{-L_A}{\sqrt{\mathbf{C}\mathbf{P}_{ss}^L\mathbf{C}^\top + R}}\right) \tag{58}$$

$$P(C_k, A_k) = P(C_k) - P(A_k') + P(C_k', A_k') \tag{59}$$

$$P(C_k', A_k') = \int_{-L_A}^{L_A}\int_{-L}^{L}\cdots\int_{-L}^{L}\mathcal{N}(\mathbf{z}; \mu_\mathbf{z}, \Sigma_\mathbf{z})d\mathbf{z} \tag{60}$$

where

$$\begin{aligned}\mathbf{z} &\triangleq \begin{bmatrix} y_k \\ \mathbf{y}_d \end{bmatrix}\\ \mu_\mathbf{z} &\triangleq \begin{bmatrix} \mu_{y_k} \\ \mu_{\mathbf{y}_d} \end{bmatrix} = \mathbf{0}_{d+1}\\ \Sigma_\mathbf{z} &\approx \begin{cases} \mathbf{C}\mathbf{P}_{ss}^L\mathbf{C}^\top + R & \forall\, i = j \in [0, \ldots, d]\\ \mathbf{C}\mathbf{A}^{j-i}\mathbf{P}_{ss}^L\mathbf{C}^\top & \forall\, j > i \in [0, \ldots, d]. \end{cases}\end{aligned}$$

The "redline" alarm system is a simple alarm level crossing used to predict a second more critical level-crossing. In this case two levels are used, L as the critical threshold, and L_A as the alarm design threshold. The "predictive" alarm system incorporates the use of predicted future process values, and defines the same envelope, $[-L_A, L_A]$, outside of which an alarm will be triggered to forewarn of the impending level-crossing event. However, the alarm definition differs from the redline method, such that $A_k = \{|\hat{y}_{k+d|k}| > L_A\}$. The predicted future process value $\hat{y}_{k+d|k}$ is derived from the standard Kalman filter (15). The probabilities necessary to compute P_d and P_{fa} based upon (34)–(35) for this alarm system are provided in (61)–(64)

$$P(A_k) = P(|\hat{y}_{k+d|k}| > L_A) \tag{61}$$

$$= 2\Phi\left(\frac{-L_A}{\sqrt{\lambda_a}}\right) \tag{62}$$

$$P(C_k, A_k) = P(C_k) - P(A_k') + P(C_k', A_k') \tag{63}$$

$$P(C_k', A_k') = \int_{-L}^{L}\cdots\int_{-L}^{L}\int_{-L_A}^{L_A}\mathcal{N}(\mathbf{z}; \mu_\mathbf{z}, \Sigma_\mathbf{z})d\mathbf{z} \tag{64}$$

where

$$\begin{aligned}\mathbf{z} &\triangleq \begin{bmatrix} \mathbf{y}_d \\ \hat{y}_{k+d|k} \end{bmatrix}\\ \mu_\mathbf{z} &\triangleq \begin{bmatrix} \mu_{\mathbf{y}_d} \\ \mu_{\hat{y}_{k+d|k}} \end{bmatrix} = \mathbf{0}_{d+1}\\ \Sigma_\mathbf{z} &\triangleq \begin{bmatrix} \Sigma_{\mathbf{y}_d} & \Lambda_a^\top \\ \Lambda_a & \lambda_a \end{bmatrix}\\ \lambda_a &= \mathbf{C}\mathbf{A}^{d-1}\left(\mathbf{P}_{ss}^L - \mathbf{P}_{ss}^R\right)(\mathbf{A}^\top)^{d-1}\mathbf{C}^\top\\ \Lambda_a &= \mathbf{C}\mathbf{A}^{d-1}\left(\mathbf{P}_{ss}^L - \mathbf{P}_{ss}^R\right)\mathbf{O}^\top.\end{aligned}$$

Note that λ_a and Λ_a have been derived with the aid of the projection theorem. All of the alarm systems described thus far will be compared using the area under the ROC curve (AUC). This provides a performance metric that characterizes the ability of each alarm system to accurately predict the level-crossing event. More precisely, it quantifies the Mann–Whitney–Wilcoxon U test statistic, which is equivalent to the probability of correctly ranking two randomly selected data points, one belonging to the level-crossing event class, the other not. The AUC has been deemed as a theoretically valid metric for model selection and algorithmic comparison [19]. The design parameters of interest are L_A for the redline and predictive methods, and P_b for the optimal alarm system and its approximations. Results will follow in the subsequent section.

III. Example

The example to be used for presentation of the results has no specific application, but is generic and based upon the same example used by Svensson *et al.* [2]. The model parameters are provided in (65)–(68)

$$\mathbf{A} = \begin{bmatrix} 0 & 1 \\ -0.9 & 1.8 \end{bmatrix} \tag{65}$$

$$\mathbf{C} = [0.5 \quad 1] \tag{66}$$

$$\mathbf{Q} = \begin{bmatrix} 0 & 0 \\ 0 & 1 \end{bmatrix} \tag{67}$$

$$R = 0.08. \tag{68}$$

Unless otherwise stated, all cases to be compared will use a threshold of $L = 16$ while varying d, or a prediction window of $d = 5$ while varying L.

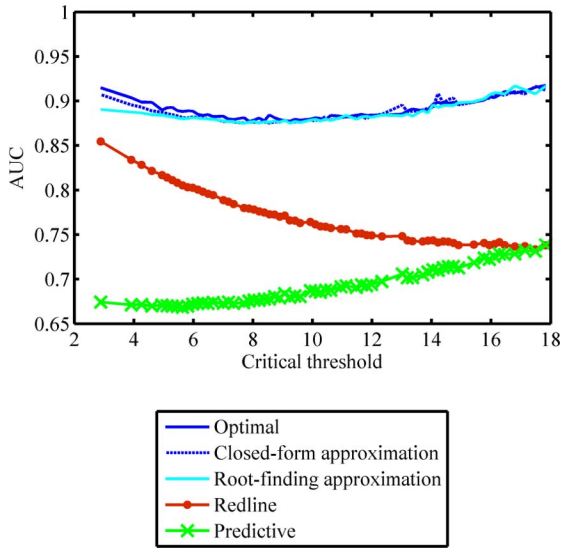

Fig. 6. AUC for all alarm systems a function of critical threshold, L.

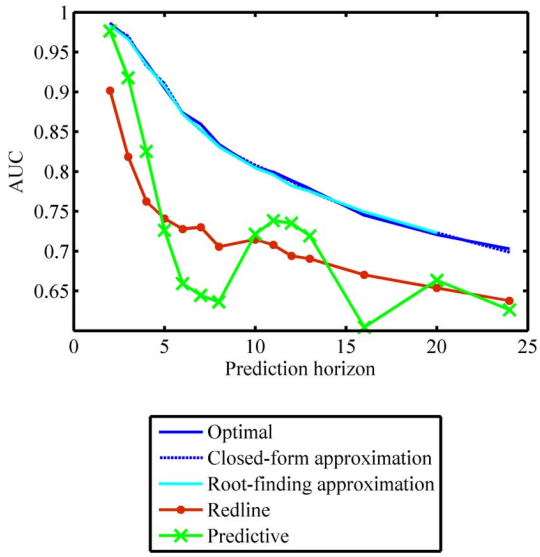

Fig. 7. AUC for all alarm systems as a function of prediction window, d.

TABLE II
EMPIRICAL ANALYSIS OF COMPUTATIONAL COMPLEXITY

	Mean Design-Time	Mean Run-Time
Optimal	81 min	9.5 msec
Closed-form	48.5 sec	0.15 msec
Root-finding	57.3 sec	0.12 msec

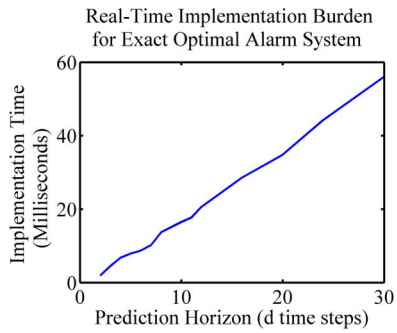

Fig. 8. Empirical run-time complexity as a function of prediction window.

IV. RESULTS AND DISCUSSION

A comparison of the AUC for all alarm systems using a prediction window of $d = 5$ while varying $L \in [2.89, 17.83]$ is shown in Fig. 6.

It is very clear that the optimal alarm system and its approximations outperform the redline and predictive methods, over the entire domain of values shown for L, as expected. Another important point to note is that the closed form and root-finding methods approximate the exact optimal performance quite well over most of the domain of values shown for L. However, as $L \to 0$, the approximation breaks down as evidenced by the notable divergence of AUC values. More careful analysis of the reasons for this divergence, including its relation to the design parameter P_b will be presented subsequently. Table II provides a summary of the empirically generated timing tests which illustrate both off-line design-time and on-line run-time computational complexity.

The second column of Table II includes the mean design time of both the redline and predictive alarm systems as well as the optimal system or its approximations across all values of L. Results presented in the row labeled ''Optimal'' were generated by Monte Carlo simulation. Clearly, there is an order of magnitude greater computational burden by using the simulation-based method of designing alarm systems to achieve a similar level of resolution in the results. Also, as expected the mean design-time for the root-finding approximation exceeds that of the closed-form approximation. As is clear by Fig. 6, there is no great loss in accuracy by using these approximations except for small values of L, where there is a perceptible, but perhaps still negligible loss.

The third column of Table II provides the mean run-time across all values of L, where it is evident again that the computational requirements of the optimal alarm condition exceed those of its approximations. In this case, the approximations involve only the time for limit checking of the type governed by (46). Thus, the actual time for root-finding is not included in the reported time for that approximation as shown in Table II, which might account for the fact that it is on par with the time for the closed form approximation. The mean run-time for checking the exact optimal alarm condition is based upon computing (23)–(24), which naturally requires more time than a simple limit check.

It is also of interest to investigate the case when using a fixed threshold of $L = 16$ while varying $d \in [2, \ldots, 24]$. A comparison of the AUC for all alarm systems for this case is shown in Fig. 7. As is clear from Fig. 7 and corroborated by Fig. 6, the optimal alarm system and its approximations outperform the redline and predictive methods as before, again over the entire domain of values shown for d. Furthermore, as the prediction window increases, the predictive performance as characterized by the AUC decreases for all alarm systems, as is to be expected. A more detailed study on the limiting effects of AUC as $d \to \infty$

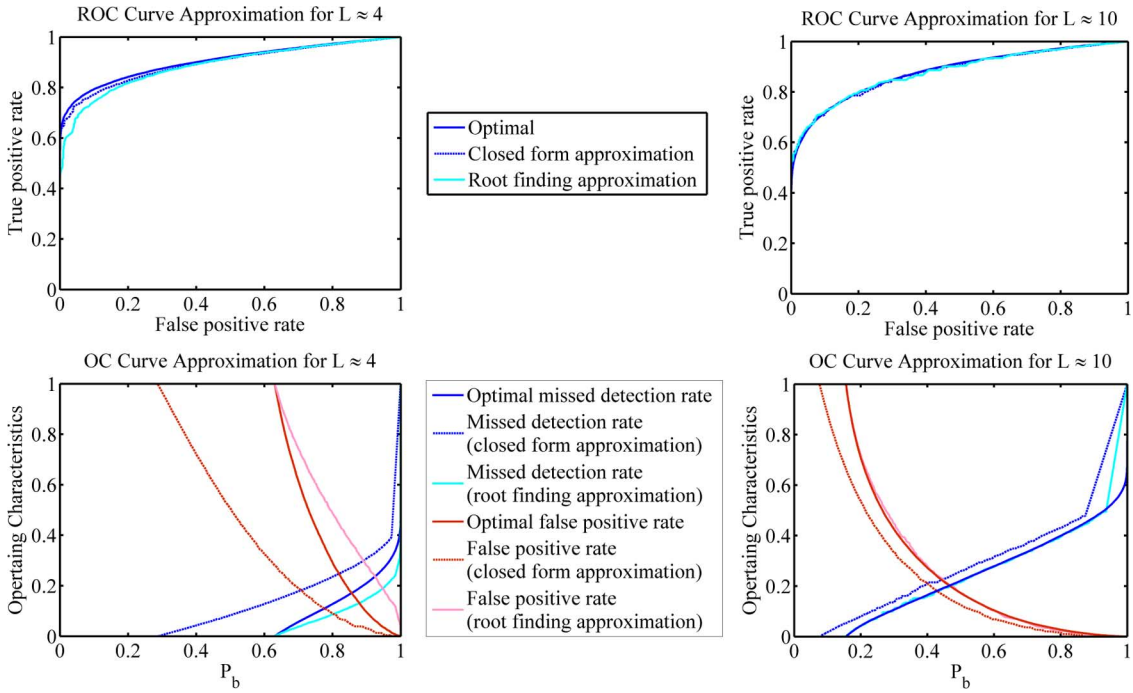

Fig. 9. ROC Curves and supporting statistics for all alarm systems, demonstrating negligible loss in accuracy for both approximations, and superiority of root-finding approximation over closed-form approximation.

will be conducted in a sequel paper. Due to the use of a modestly large fixed threshold of $L = 16$, however, there are no deleterious effects as a result of using approximations to the optimal alarm system as were found when investigating the case when varying L to small values.

Characterization of complexity as d increases is also of interest. For the most part, the results are very similar to what was presented in Table II for the case in which a prediction window of $d = 5$ was used while varying L. Specifically, the mean design time for the exact optimal alarm system (along with redline and predictive alarm systems) was on par with what was shown in Table II (74 min in lieu of 81 min). However, the run-time in this case increases linearly as shown in Fig. 8.

As the prediction window increases, the runtime for checking the exact optimal alarm condition based upon computing (23) and (24) naturally requires more time for larger prediction horizons. A key advantage in using approximations can therefore be realized. For both the closed form and root finding approximations, the mean runtime is exactly on par with what was presented in Table II for the case in which a prediction window of $d = 5$ was used while varying L (averaging 0.11 ms). This is primarily due to the fact that, again, runtime for the approximations involve only limit checking of the type governed by (46).

As for the design time of the approximations, they too exhibit similar characteristics to what was presented and discussed in conjunction with Table II. Specifically, there is a general upward trend of the design time (which again include design times for both the redline and predictive alarm systems) as d increases. The mean design times are moderately higher than what was presented in Table II (111 s in lieu of 44.2 s for the closed-form approximation and 129 s in lieu of 55.2 s for the root-finding approximation).

Recall the notable divergence in AUC values between the exact and optimal alarm approximations, which break down as $L \to 0$, shown in Fig. 6. Insight for the origins of this divergence may be derived from examination of a candidate ROC curve corresponding to a small value of L. In Fig. 9, it can be visually discerned how both approximations break down as related to the design parameter P_b for a small value of $L \approx 4$ compared to a larger value of $L \approx 10$.

The topmost panels of the figure illustrate ROC curves corresponding to the different values of L. For the optimal alarm system shown in the top left panel, the two approximations yield ROC curves that are close but not identical to the exact optimal result when $L \approx 4$. On the top right panel when $L \approx 10$, the ROC curve approximations appear to be much closer than on the top left panel where $L \approx 4$. This substantiates a previous observation made from Fig. 6, that as L decreases, the approximation loses its accuracy. Furthermore, from the previous section, Figs. 2 and 5 showed the optimal alarm regions and their approximations to provide further evidence of this loss of accuracy as L decreases. Those figures were based upon the same example used to generate the results presented in this section.

Further insight can be gained by inspecting the bottom two panels of Fig. 9 as well. Note that the bottom panels show the missed detection and false positive rates as a function of P_b. The complement of the former is the true positive rate, which along with the false positive rate, is used to construct the ROC curves shown on the top panels. It is evident that the closed form approximations to the optimal alarm system yield true and false positive rates that are systematically underreported for both values of L shown. This corroborates the mathematical observation made from the previous section based upon the containment relationship of the closed form approximation to

the exact optimal alarm region, $\bigcup_{j=1}^{d}\bigcup_{i\in\mathcal{B}}A_k^{i,j}\subseteq\bigcup_{j=1}^{d}A_k^j\subseteq A_k$. For the smaller value of $L\approx 4$, this underreporting of the true and false positive rates is even more striking than for the larger value of $L\approx 10$.

Furthermore, the root finding approximations to the optimal alarm system yield true and false positive rates that are overreported for both values of L shown. This is much more clear for the smaller value of $L\approx 4$ than for the larger value of $L\approx 10$. Hence, again this corroborates an inference made from mathematical observations made in the previous section. Recall the containment relationship between the root finding and closed form approximation to the exact optimal alarm region $\bigcup_{j=1}^{d}A_k^j\subseteq\bigcup_{j=1}^{d}\Omega_{A_j}$. It was suggested that the root finding approximation strategy may be overly aggressive and overshoot the performance of the exact optimal method under certain circumstances. This is clear for the smaller value of $L\approx 4$.

There is one last important note about the root finding approximations that is evident in the bottom two panels of Fig. 9. The feasible domain of values for P_b is identical to the exact optimal alarm region of feasibility, which was also proven mathematically in the previous section. The same is not true for the closed form approximation, where the region of feasibility is clearly different, and drastically so for the smaller value of $L\approx 4$.

V. Conclusions and Future Work

In this paper, a novel state-space approach to the optimal alarm systems literature has been introduced, which also contributes to the Kalman filter-based fault detection literature from a different theoretical angle. In doing so, it has been demonstrated that there is a negligible loss in overall accuracy when using approximations to the theoretically optimal level-crossing predictor for a stationary linear Gaussian process, at the advantage of greatly reduced computational complexity. The negligibility of the loss in accuracy was demonstrated by comparing two approximations of the optimal level-crossing predictor to two competing methods. Both approximations clearly outperformed the two competing methods over various domains for both L and d. However, care should be taken when designing alarm systems for which level-crossing events are defined with small values of L. Specifically, when using approximations, alarm system design should be governed both by ROC curve analysis as well as supporting false positive or missed detection rate statistics parameterized by the design parameter P_b.

In future work, the limiting effects of AUC for the closed-form approximation introduced in this paper will be investigated. Specifically, limiting values for relevant statistics as L, R, and d approach the extremities of their feasible domains will be examined. Doing so will help to facilitate a new and broader context for the design of an optimal alarm system related to important engineering design parameters. Furthermore, control theoretic implications and ramifications of using the Kalman filter in tandem with optimal alarm theory that naturally follow will be investigated. Here, it will also be possible to gain further insight into important engineering design considerations for both the analysis and synthesis of algorithms used for mitigation of potential adverse events from a practical standpoint. Relaxing some of the inherent assumptions made in this paper to the point where nonparametric methods such as Gaussian process regression and particle filtering are accessible may also provide a natural vehicle for the extension of optimal alarm theory to other machine learning research domains. Finally, extension of this work to systems containing both multivariate inputs and outputs is important, and has practical appeal to the field of data mining. As such, scalability and complexity will remain important considerations.

VI. Acknowledgements

The author would like to thank Prof. D. Auslander of the Mechanical Engineering Department, University of California, Berkeley, and Dr. C. Federspiel for guidance and advocacy during the completion of his Ph.D. degree in conducting applied research related to this topic during its conception. The author would also like to thank Dr. M. Schwabacher, Dr. N. Oza, D. McIntosh, J. Wallerius, and Dr. S. Das for reviewing various versions of this paper throughout its evolution. Finally, the author would like to thank the reviewers selected by the editorial board of the IEEE Transactions on Information Theory for important points they made and for their valuable comments and criticisms which greatly helped to allow for the development of a more technically sound article.

VII. Theorems and Lemmas

Theorem 1: From (1)–(3), it is clear that successive output values of the stationary stochastic process, y_k admit a well-defined jointly Gaussian probability density function. Also, the level-crossing event, C_k, defined through (4), represents at least one exceedance outside of the threshold envelope specified by $[-L,L]$ of the process y_k. Then the optimal level-crossing predictor can be written as $P(C_k|y_0,\ldots,y_k)\geq P_b$, where the condition for optimality is as specified and defined by the use of the likelihood ratio criterion in (69) as a result of the Neyman–Pearson Lemma, shown by DeMaré [6], and more explicitly by Lindgren [7], [20]

$$\frac{p(y_0,\ldots,y_k|C_k')}{p(y_0,\ldots,y_k|C_k)}\leq\lambda. \tag{69}$$

Proof: Using Lemma 1,[1] we can rewrite (69) as follows:

$$\begin{aligned}
&\frac{p\left(y_0,\ldots,y_k|C_k'\right)}{p(y_0,\ldots,y_k|C_k)}\leq\lambda\\
&\frac{\frac{P(C_k'|y_0,\ldots,y_k)\cancel{p(y_0,\ldots,y_k)}}{P(C_k')}}{\frac{P(C_k|y_0,\ldots,y_k)\cancel{p(y_0,\ldots,y_k)}}{P(C_k)}}\leq\lambda\\
&\frac{P(C_k'|y_0,\ldots,y_k)P(C_k)}{P(C_k|y_0,\ldots,y_k)P(C_k')}\leq\lambda.
\end{aligned}$$

However, due to the assumption of stationarity of the process, the size of the alarm region, $P(C_k)$, associated with the uniformly most powerful test of the hypothesis $\mathcal{H}_0$ is by definition a constant value. The hypothesis being tested in this case is of

[1]Which curiously appears very much like Bayes' rule, but can be distinguished from it due to the use of both probabilities and density functions.

the level-crossing event, C_k. Due to the size of alarm region being fixed, we can define new constants as shown below

$$\begin{aligned}\frac{1-P(C_k|y_0,\ldots,y_k)}{P(C_k|y_0,\ldots,y_k)} &\leq \lambda\frac{P(C_k')}{P(C_k)} \triangleq \gamma\\ P(C_k|y_0,\ldots,y_k) &\geq \frac{1}{1+\gamma} \triangleq P_b\\ \Leftrightarrow P(C_k|y_0,\ldots,y_k) &\geq P_b.\end{aligned}$$

■

Lemma 1:

$$p(y_0,\ldots,y_k|C_k) = \frac{P(C_k|y_0,\ldots,y_k)p(y_0,\ldots,y_k)}{P(C_k)}. \quad (70)$$

Proof:

$$\begin{aligned}p(y_0,\ldots,y_k|C_k) &\triangleq \frac{\int\cdots\int_{\Omega_C} p(y_0,\ldots,y_{k+d})d\mathbf{y}_d}{P(C_k)}\\ &= \frac{\int\cdots\int_{\Omega_C} p(y_0,\ldots,y_{k+d})d\mathbf{y}_d}{p(y_0,\ldots,y_k)}\\ &\quad\cdot\frac{p(y_0,\ldots,y_k)}{P(C_k)}\\ &= \frac{P(C_k|y_0,\ldots,y_k)p(y_0,\ldots,y_k)}{P(C_k)}\end{aligned}$$

where by definition $P(C_k|y_0,\ldots,y_k) \triangleq$

$$\int\cdots\int_{\Omega_C} p(y_{k+1},\ldots,y_{k+d}|y_0,\ldots,y_k)d\mathbf{y}_d = \frac{\int\cdots\int_{\Omega_C} p(y_0,\ldots,y_{k+d})d\mathbf{y}_d}{p(y_0,\ldots,y_k)}$$

and

$$\Omega_C = \left\{\mathbf{y}_d\in\mathbb{R}^d : C_k \triangleq \bigcup_{j=1}^{d} S_{k+j}\right\}.$$

■

Lemma 2:

$$P_{b_d} = \max_j P_{b_j} \Updownarrow V_{k+j+1|k} > V_{k+j|k},\ \forall\, j\in[1,\ldots,d].$$

Proof: The posited claim is true *iff*

$$P_{b_1} < \cdots < P_{b_j} < P_{b_{j+1}} < \cdots < P_{b_d}.$$

More compactly

$$P_{b_j} < P_{b_{j+1}},\ \forall\, j\in[1,\ldots,d].$$

The following chain of inequalities is true $\forall\, j\in[1,\ldots,d]$

$$\begin{aligned}P_{b_j} &< P_{b_{j+1}}\\ \Phi^{-1}(P_{b_j}) &< \Phi^{-1}(P_{b_{j+1}})\\ \left(\frac{-L}{\Phi^{-1}(P_{b_{j+1}})}\right)^2 &> \left(\frac{-L}{\Phi^{-1}(P_{b_j})}\right)^2\\ V_{k+j+1|k} &> V_{k+j|k}.\end{aligned}$$

■

Lemma 3:

$$\mathbf{P}_{ss}^R \succeq \hat{\mathbf{P}}_{ss}^R \Downarrow V_{k+j+1|k} > V_{k+j|k},\ \forall\, j\in[1,\ldots,d].$$

Proof:

$$\begin{aligned}\mathbf{P}_{ss}^R &\succeq \hat{\mathbf{P}}_{ss}^R\\ \mathbf{P}_{ss}^R - \hat{\mathbf{P}}_{ss}^R &\succeq 0\\ \mathbf{x}^\top\left(\mathbf{P}_{ss}^R - \hat{\mathbf{P}}_{ss}^R\right)\mathbf{x} &\geq 0,\ \forall\,\mathbf{x}\in\mathbb{R}^n\\ \mathbf{x}^\top\left(\hat{\mathbf{P}}_{ss}^R + \mathbf{Q} - \mathbf{P}_{ss}^R\right)\mathbf{x} &\leq \mathbf{x}^\top\mathbf{Q}\mathbf{x},\ \forall\,\mathbf{x}\in\mathbb{R}^n.\end{aligned}$$

By using the steady-state version of (13) and the discrete algebraic Lyapunov equation we now have the following, $\forall\,\mathbf{x}\in\mathbb{R}^n$:

$$\begin{aligned}\mathbf{x}^\top\left(\hat{\mathbf{P}}_{ss}^R - \mathbf{A}\hat{\mathbf{P}}_{ss}^R\mathbf{A}^\top\right)\mathbf{x} &\leq \mathbf{x}^\top\left(\mathbf{P}_{ss}^L - \mathbf{A}\mathbf{P}_{ss}^L\mathbf{A}^\top\right)\mathbf{x}\\ \mathbf{x}^\top\left(\hat{\mathbf{P}}_{ss}^R - \mathbf{P}_{ss}^L\right)\mathbf{x} &\leq \mathbf{x}^\top\mathbf{A}\left(\hat{\mathbf{P}}_{ss}^R - \mathbf{P}_{ss}^L\right)\mathbf{A}^\top\mathbf{x}.\end{aligned}$$

Let $\mathbf{x}^\top \triangleq \mathbf{C}\mathbf{A}^j$, $\forall\, j\in[1,\ldots,d]$, and add $\mathbf{C}\mathbf{P}_{ss}^L\mathbf{C}^\top + R$ to both sides of the inequality above. It then follows that the following relations hold true, $\forall\, j\in[1,\ldots,d]$

$$\begin{aligned}\mathbf{C}\mathbf{P}_{k+j|k}\mathbf{C}^\top + R &\leq \mathbf{C}\mathbf{P}_{k+j+1|k}\mathbf{C}^\top + R\\ V_{k+j+1|k} &> V_{k+j|k}.\end{aligned}$$

■

Lemma 4: $R>0 \Rightarrow \mathbf{P}_{ss}^R \succeq \hat{\mathbf{P}}_{ss}^R$

Proof: It is true that

$$R>0 \Leftrightarrow R^{-1}>0.$$

Under the condition that $\mathbf{C}\in\mathbb{R}^{1\times n}$, where $n>1$, with no rank condition on $\mathbf{C}$, Lemma 5 can be used to support the following implication:

$$R^{-1}>0 \Rightarrow \mathbf{C}^\top R^{-1}\mathbf{C} \succeq 0.$$

Also, given the matrix inversion lemma applied to (20) shown below, the subsequent series of equations proves that $\mathbf{P}_{ss}^{R} \succeq \hat{\mathbf{P}}_{ss}^{R}$

$$\begin{aligned}
\hat{\mathbf{P}}_{ss}^{R} &= \mathbf{P}_{ss}^{R} - \mathbf{P}_{ss}^{R}\mathbf{C}^{\top}\left(\mathbf{C}\mathbf{P}_{ss}^{R}\mathbf{C}^{\top} + R\right)^{-1}\mathbf{C}\mathbf{P}_{ss}^{R} \\
&\overset{M.I.L}{=} \left[\left(\mathbf{P}_{ss}^{R}\right)^{-1} + \mathbf{C}^{\top}R^{-1}\mathbf{C}\right]^{-1} \\
\therefore \left(\hat{\mathbf{P}}_{ss}^{R}\right)^{-1} &= \left(\mathbf{P}_{ss}^{R}\right)^{-1} + \mathbf{C}^{\top}R^{-1}\mathbf{C} \\
\mathbf{C}^{\top}R^{-1}\mathbf{C} &\succeq 0 \\
\left(\hat{\mathbf{P}}_{ss}^{R}\right)^{-1} - \left(\mathbf{P}_{ss}^{R}\right)^{-1} &\succeq 0 \\
\left(\hat{\mathbf{P}}_{ss}^{R}\right)^{-1} &\succeq \left(\mathbf{P}_{ss}^{R}\right)^{-1} \\
\mathbf{P}_{ss}^{R} &\succeq \hat{\mathbf{P}}_{ss}^{R}.
\end{aligned}$$

■

Lemma 5: Given $\mathbf{L} \in \mathbb{R}^{n\times d}$, for which $d > n$ and there exists no rank condition on $\mathbf{L}$: $\mathbf{M} \succ 0 \Rightarrow \mathbf{L}^{\top}\mathbf{M}\mathbf{L} \succeq 0$.

Proof:

$$\begin{aligned}
\mathbf{M} &\succeq 0 \\
\therefore \mathbf{x}^{\top}\mathbf{M}\mathbf{x} &\geq 0, \forall\, \mathbf{x} \in \mathbb{R}^{n} \\
\mathbf{x} &\triangleq \mathbf{L}\mathbf{y} \\
Null(\mathbf{L}) &\triangleq \{\mathbf{y} : \mathbf{L}\mathbf{y} = 0\} \\
\dim Null(\mathbf{L}) &\geq d - n > 0 \\
\exists \mathbf{y} : &\mathbf{L}\mathbf{y} = 0 \\
\mathbf{y}^{\top}\mathbf{L}^{\top}\mathbf{M}\mathbf{L}\mathbf{y} &\geq 0, \forall\, \mathbf{x} \in \mathbb{R}^{n} \\
\mathbf{L}^{\top}\mathbf{M}\mathbf{L} &\succeq 0.
\end{aligned}$$

■

REFERENCES

[1] A. Svensson, "Event Prediction and Bootstrap in Time Series," Ph.D., Lund Inst. Technol., Lund, 1998.

[2] A. Svensson, J. Holst, R. Lindquist, and G. Lindgren, "Optimal prediction of catastrophes in autoregressive moving-average processes," *J. Time Ser. Anal.*, vol. 17, no. 5, pp. 511–531, 1996.

[3] R. A. Martin, "Optimal Prediction, Alarm, and Control in Buildings Using Thermal Sensation Complaints," Ph.D. dissertation, Univ. California, Berkeley, 2004.

[4] H. Grage, J. Holst, G. Lindgren, and M. Saklak, "Level crossing prediction with neural networks," presented at the Methodology and Computing in Applied Probability, 2009 [Online]. Available: http://dx.doi.org/10.1007/s11009-009-9153-3

[5] S.-I. Beckman, J. Holst, and G. Lindgren, "Alarm characteristics for a flood warning system with deterministic components," *J. Time Series Anal.*, vol. 11, no. 1, pp. 1–18, Mar. 1987.

[6] J. DeMaré, "Optimal prediction of catastrophes with application to Gaussian processes," *Ann. Probab.*, vol. 8, no. 4, pp. 840–850, Aug. 1980.

[7] G. Lindgren, "Optimal prediction of level crossings in Gaussian processes and sequences," *Ann. Probab.*, vol. 13, no. 3, pp. 804–824, Aug. 1985.

[8] T. H. Kerr, "False alarm and correct detection probabilities over a time interval for restricted classes of failure detection algorithms," *IEEE Trans. Inf. Theory*, vol. IT-28, no. 7, pp. 619–631, Jul. 1982.

[9] J. P. Butas, L. M. Santi, and R. B. Aguilar, "A tiered approach to J-2X health and status monitoring," presented at the 54th Joint Army-Navy-NASA-Air Force Propulsion Meet., 2007.

[10] M. Basseville and I. V. Nikiforov, *Detection of Abrupt Changes: Theory and Application*. Upper Saddle River, NJ: Prentice-Hall, 1993.

[11] A. S. Willsky and H. L. Jones, "A generalized likelihood ratio approach to the detection and estimation of jumps in linear systems," *IEEE Trans. Autom. Control*, vol. 21, pp. 108–112, 1976.

[12] D. J. Pedregal and M. C. Carnero, "State space models for condition monitoring: A case study," *Rel. Eng. Syst. Safety*, vol. 91, no. 2, pp. 171–180, 2006.

[13] M. Antunes, A. A. Turkman, and K. F. Turkman, "A Bayesian approach to event prediction," *J. Time Ser. Anal.*, vol. 24, no. 6, pp. 631–646, Nov. 2003.

[14] N. H. Pontoppidan and J. Larsen, "Unsupervised condition change detection in large diesel engines," in *Proc. 13th IEEE Workshop on Neural Networks for Signal Processing*, Sep. 2003, pp. 565–574.

[15] R. Bickford, MSET Signal Validation System Final Report 2000, NASA Contract NAS8-98027, Tech. Rep..

[16] F. Lewis, *Applied Optimal Control & Estimation: Digital Design & Implementation*. Upper Saddle River, NJ: Prentice-Hall, 1992.

[17] A. Genz, "Numerical computation of multivariate normal probabilities," *J. Comput. Graph. Statist.*, vol. 1, pp. 141–149, 1992.

[18] T. H. Kerr, III, "Integral evaluations enabling performance tradeoffs for two-confidence-region-based failure detection," *J. Guid., Control, Dyn.*, vol. 29, no. 3, pp. 757–762, May–Jun. 2006.

[19] A. P. Bradley, "The use of the area under the ROC curve in the evaluation of machine learning algorithms," *Pattern Recognit.*, vol. 30, no. 7, pp. 1145–1159, 1997.

[20] G. Lindgren, "Model processes in nonlinear prediction with application to detection and alarm," *Ann. Probab.*, vol. 8, no. 4, pp. 775–792, Aug. 1980.

Rodney A. Martin (M'02) received the B.S. degree in mechanical engineering from Carnegie-Mellon University, Pittsburgh, PA, in 1992, the M.S. and Ph.D. degrees in mechanical engineering from the University of California, Berkeley, in 2000 and 2004, respectively.

He spent nearly five years on active duty as a Naval Officer in the U.S. Navy prior to entering graduate school and has worked as a Computer Engineer at NASA Ames Research Center since completing his Ph.D. degree in 2004. His research interests span the areas of fault detection, estimation, prediction, control theory, and machine learning. Most recently, he has worked on applying techniques from these research areas to projects at NASA that address aviation safety and space propulsion systems.

Dr. Martin is currently a member of AIAA.

Corrections

Errata for "A State-Space Approach to Optimal Level-Crossing Prediction for Linear Gaussian Processes"

Rodney A. Martin, *Member, IEEE*

1) In [1], on p. 5086, Column 1, under Eq. 14, the definition for $\mathbf{P}_{k|k}$ should include a $^\top$ for the transpose operator, not ^{T}, as such

$$\mathbf{P}_{k|k} \triangleq E[(\mathbf{x}_k - \hat{\mathbf{x}}_{k|k})(\mathbf{x}_k - \hat{\mathbf{x}}_{k|k})^\top | y_0, \ldots, y_k].$$

2) On p. 5088, Column 1, Eq. 34, should be revised as follows:

True positive rate:

$$P_d = P(A_k|C_k) = \frac{P(C_k, A_k)}{P(C_k)}.$$

3) On p. 5088, Column 1, under Eq. 37, the integral defined for $P(A_k^{'})$ should be with respect to $d\hat{\mathbf{y}}_d$ in lieu of $d\mathbf{y}_d$, as such

$$P(A_k^{'}) = P(\bigcap_{j=1}^{d} \Omega_{A_j}^{'}) = P(\bigcap_{j=1}^{d} |\hat{y}_{k+j|k}| < L_{A_j})$$
$$= \int_{-L_{A_1}}^{L_{A_1}} \cdots \int_{-L_{A_d}}^{L_{A_d}} \mathcal{N}(\hat{\mathbf{y}}_d; \mu_{\mathbf{y}_d}, \hat{\Sigma}_{\hat{\mathbf{y}}_d}) d\hat{\mathbf{y}}_d.$$

4) On p. 5090, Column 2, Eqs. 53–56, the mean of the normal distribution associated with each of the corresponding integrals should be $\mathbf{0}_d$, not $\hat{\mathbf{y}}_d$, as follows:

$$f(\hat{y}_{k+j|k}) = \lim_{\hat{\mathbf{y}}_d \setminus \hat{y}_{k+j|k} \to \mu_{\mathbf{y}_d} \setminus \mu_{y_{k+j}}} P(\bigcap_{j=1}^{d} E_{k+j}|y_0, \ldots, y_k)$$
$$= \int_{\mathcal{D}_\Omega} \mathcal{N}(\mathbf{y}_d; \mathbf{0}_d, \hat{\Sigma}_{\mathbf{y}_d}) d\mathbf{y}_d$$
$$= \int_{-L}^{L} \cdots \int_{-L-\hat{y}_{k+j|k}}^{L-\hat{y}_{k+j|k}} \cdots \int_{-L}^{L} \mathcal{N}(\mathbf{y}_d; \mathbf{0}_d, \hat{\Sigma}_{\mathbf{y}_d}) d\mathbf{y}_d$$
$$P(E_{k+j}|y_0, \ldots, y_k) = \int_{\mathcal{D}_A} \mathcal{N}(\mathbf{y}_d; \mathbf{0}_d, \hat{\Sigma}_{\mathbf{y}_d}) d\mathbf{y}_d$$
$$= \int_{-\infty}^{\infty} \cdots \int_{-L-\hat{y}_{k+j|k}}^{L-\hat{y}_{k+j|k}} \cdots \int_{-\infty}^{\infty} \mathcal{N}(\mathbf{y}_d; \mathbf{0}_d, \hat{\Sigma}_{\mathbf{y}_d}) d\mathbf{y}_d.$$

Manuscript received June 08, 2011; accepted June 14, 2011. Date of current version November 11, 2011. This work was supported in part by the Integrated Vehicle Health Management (IVHM) project, funded by the Aviation Safety Program of NASA's Aeronautics Research Mission Directorate.

The author is with the Intelligent Systems Division and the Intelligent Data Understanding Group, NASA Ames Research Center, Moffett Field, CA 94035 USA (e-mail: rodney.martin@nasa.gov).

Digital Object Identifier 10.1109/TIT.2011.2160614

References

[1] R. A. Martin, "A state-space approach to optimal level-crossing prediction for linear Gaussian processes," *IEEE Trans. Inf. Theory*, vol. 56, no. 10, pp. 5083–5096, Oct. 2010.

Rodney A. Martin (M'02) received the B.S. degree in mechanical engineering from Carnegie-Mellon University, Pittsburgh, PA, in 1992, and the M.S. and Ph.D. degrees, both in mechanical engineering, from the University of California, Berkeley, in 2000 and 2004, respectively.

He spent nearly five years on active duty as a Naval Officer in the U.S. Navy prior to entering graduate school, and has worked as a Computer Engineer at NASA Ames Research Center since completing his Ph.D. degree in 2004. His research interests span the areas of fault detection, estimation, prediction, control theory, and machine learning. Most recently he has worked on applying techniques from these research areas to projects at NASA that address aviation safety and space propulsion systems.

Dr. Martin is a member of AIAA.

U.S. Government work not protected by U.S. copyright.